pISSN 1598-2033
eISSN 2233-5706

Journal of the Korea Institute of Building Construction, Vol. 14, No. 3
http://dx.doi.org/10.5345/JKIBC.2014.14.3.273

www.jkibc.org

# Modeling of temperature history in the hardening of ultra-high-performance concrete

**Wang, Xiao-Yong***

*Department of Architectural Engineering, College of Engineering, Kangwon National University, Chuncheon, 200-701, Korea*

**Abstract**

Ultra-high-performance concrete (UHPC) consists of cement, silica fume (SF), sand, fibers, water and superplasticizer. Typical water/binder ratios are 0.15 to 0.20 with 20 to 30% silica fume. In the production of ultra-high performance concrete, a significant temperature rise at an early age can be observed because of the higher cement content per unit mass of concrete. In this paper, by considering the production of calcium hydroxide in cement hydration and its consumption in the pozzolanic reaction, a numerical model is proposed to simulate the hydration of ultra-high performance concrete. The heat evolution rate of UHPC is determined from the contributions of cement hydration and the pozzolanic reaction. Furthermore, by combining a blended-cement hydration model with the finite-element method, the temperature history in the hardening of UHPC is evaluated using the degree of hydration of the cement and the silica fume. The predicted temperature-history curves were compared with experimental data, and a good correlation was found.

Keywords : ultra-high performance concrete, hydration heat, early-age temperature history, hydration model, finite-element method

## 1. Introduction

Ultra-high-performance concrete (UHPC) consists of cement, silica fume (SF), sand, fibers, water and superplasticizer. Typical water/binder ratios are 0.15 to 0.20 with 20 to 30% silica fume. The mechanical properties of UHPC include a compressive strength greater than 150MPa and a sustained post-cracking tensile strength greater than 5MPa. UHPC has a discontinuous pore structure that reduces liquid ingress, significantly enhancing its durability compared with that of conventional and high-performance concretes[1].

For ultra-high performance concrete, a significant temperature rise at an early age can be observed because of the higher cement content per unit mass of concrete. This can jeopardize the durability and the appearance of the concrete members due to early-age cracking. A cogent simulation of the exothermic hydration process of cements plays a crucial role in quantifying the thermal stress and assessing the risk probability of thermal cracking in mass-concrete structures. In the past, several researchers[2,3,4,5,6,7] have attempted to predict the temperature rise in hardening concrete, but these models are not valid for ultra-high performance concrete, which has a much lower water-to-binder ratio and a higher silica-fume content. The shortcomings of these hydration heat

Received : February 10, 2014
Revision received : April 3, 2014
Accepted : April 11, 2014
* Corresponding author : Wang Xiao-Yong
[Tel: 82-33-250-6229, E-mail: wxbrave@kangwon.ac.kr]

models are as follows. First, the focus of the proposed models[2,3] has been on tracking the relationships between the hydration-heat rate and the concrete-maturity function under adiabatic conditions. The models did not consider the effect of the water-to-cement ratio (w/c) on hydration-heat release and the influence of the reaction temperature on the rate of hydration. Second, the proposed models[4,5] have evaluated the temperature history using a cement-hydration model. However, these models[4,5] were only valid for Portland-cement concrete, and more improvements are needed to consider the pozzolanic reaction of silica fume. Third, the proposed models[6,7] have considered both Portland-cement hydration and the reaction of mineral admixtures. However, these models[6,7] were only valid for normal-strength concrete, and require additional modifications to predict the temperature history of ultra-high-strength concrete.

In this paper, to predict the temperature distribution in ultra-high-performance concrete, we propose a blended-cement-hydration model that takes the effect of temperature on the rate of cement hydration into account. The heat evolution rate of UHPC is determined from the contribution of the cement-hydration reaction and the pozzolanic reaction. In addition, a finite-element analysis considering the temperature-dependent heat production is performed to evaluate the temperature history and distribution in concrete.

The contributions of this paper are as follows. First, the proposed hydration model has taken into account both the hydration of Portland cement and the pozzolanic reaction of silica fume. Second, the proposed hydration model has considered the influences of the water-to-binder ratio, the silica-fume-replacement ratio and the curing temperature on the hydration rate, and is valid for both ordinary-strength concrete and ultra-high-strength concrete. Third, in the finite-element modeling process, the proposed model analyzes the difference in the heat-evolution rate between the surface part and the central part in the hardening concrete.

## 2. Blended-cement hydration model

### 2.1 Portland-cement hydration model

The shrinking-core model, which was originally developed by Tomosawa[8], is used in this study to simulate the development of cement hydration. This model is expressed as a single equation consisting of three coefficients: $k_d$, the reaction coefficient in the induction period; $D_e$, the effective diffusion coefficient of water through the C-S-H gel; and $k_{ri}$, a coefficient of the reaction rate of the mineral compound of cements, as shown in Eqs. (1-1) and (1-2) below:

$$\frac{d\alpha_i}{dt} = \frac{3(S_w / S_0)\rho_w C_{w-free}}{(\nu + w_g) r_0 \rho_c} \quad \text{---------- (1-1)}$$

$$, \quad \frac{1}{(\frac{1}{k_d} - \frac{r_0}{D_e}) + \frac{r_0}{D_e}(1-\alpha_i)^{\frac{-1}{3}} + \frac{1}{k_{ri}}(1-\alpha_i)^{\frac{-2}{3}}} \quad \text{---- (1-2)}$$

where $\alpha_i$ ($i$=1,2,3 and 4) represents the reaction degree of the mineral compounds of cement, $C_3S$, $C_2S$, $C_3A$ and $C_4AF$, respectively; $\alpha$ is the degree of cement hydration and can be calculated from the weight fraction of the mineral compounds $g_i$ and the reaction degree of the mineral compounds $\alpha_i$; $\nu$ is the stoichiometric ratio by mass of water to cement (= 0.25); $w_g$ is the physically bound water in the C-S-H gel (= 0.15); $\rho_w$ is the density of water; $\rho_c$ is the density of the cement; $C_{w-free}$ is the amount

of water at the exterior of the C-S-H gel; $r_0$ is the radius of the unhydrated cement particles; $S_w$ is the effective surface area of the cement particles in contact with water; and $S_0$ is the total surface area if the surface area develops unconstrained.

The reaction coefficient $k_d$ is assumed to be a function of the degree of hydration, as shown in eq. (2) where $B$ and $C$ are the coefficients determining this factor; $B$ controls the rate of the initial shell formation and $C$ controls the rate of the initial shell decay.

$$k_d = \frac{B}{\alpha^{1.5}} + C\alpha^3 \quad \text{---------- (2)}$$

The effective diffusion coefficient of water is affected by the tortuosity of the gel pores as well as the radii of the gel pores in the hydrate. This phenomenon can be described as a function of the degree of hydration, and is expressed as follows:

$$D_e = D_{e0} \ln(\frac{1}{\alpha}) \quad \text{---------- (3)}$$

The amount of water in the capillary pores $C_{w-free}$ is expressed as a function of the degree of hydration in the previous step, as shown in Eq. (4):

$$C_{w-free} = \left( \frac{W_0 - 0.4C_0\alpha}{W_0} \right)^r \quad \text{---------- (4)}$$

where $C_0$ and $W_0$ are the mass fractions of cement and water in the mix proportion, respectively, and $r$ is an empirical parameter considering the accessibility of water into the inner, anhydrous part through an outer, hard shell of the cement particles[8].

The effect of temperature on these reaction coefficients is assumed to follow the Arrhenius law, as shown in Eqs. (5)-(8):

$$B = B_{20} \exp(-\beta_1(\frac{1}{T} - \frac{1}{293})) \quad \text{---------- (5)}$$

$$C = C_{20} \exp(-\beta_2(\frac{1}{T} - \frac{1}{293})) \quad \text{---------- (6)}$$

$$k_{ri} = k_{ri20} \exp(-\frac{E}{R}(\frac{1}{T} - \frac{1}{293})) \quad \text{---------- (7)}$$

$$D_e = D_{e20} \exp(-\beta_3(\frac{1}{T} - \frac{1}{293})) \quad \text{---------- (8)}$$

where $\beta_1$, $\beta_2$, $E/R$ and $\beta_3$ are temperature-sensitivity coefficients, and $B_{20}$, $C_{20}$, $k_{ri20}$ and $D_{e20}$ are the values of $B$, $C$, $k_{ri}$ and $D_e$ at 20 ℃, respectively.

On the basis of the degree of the reactions of the mineral compounds of cement[9], the parameters of the hydration model are calibrated and shown in Table 1. These parameters do not vary with the water-to-cement ratios and the cement-mineral compositions. When the water-to-cement ratio, the cement-mineral compositions, the cement Blaine surface and the curing temperature are given, the model can automatically determine the degree of cement hydration.

### 2.2 Silica-fume-reaction model

Based on an analysis of the experimental results regarding the amount of chemically bound water, the increase in the adiabatic temperature and the measured temperature of small quasi-adiabatic blocks, Maekawa[10] and Lura[11] stated that the reaction of silica fume can be roughly described by

Table 1. Coefficients of the cement-hydration model

| $B_{20}$ (cm/h) | $C_{20}$ (cm/h) | $k_{rC_3S20}$ (cm/h) | $k_{rC_2S20}$ (cm/h) | $k_{rC_3A20}$ (cm/h) | $k_{rC_4AF20}$ (cm/h) | $D_{e20}$ ($cm^2$/h) | $\beta_1$ (K) | $\beta_2$ (K) | $\beta_3$ (K) | $\frac{E}{R}$ (K) |
|---|---|---|---|---|---|---|---|---|---|---|
| $8.09\times10^{-9}$ | 0.02 | $9.03\times10^{-6}$ | $2.71\times10^{-7}$ | $1.35\times10^{-6}$ | $6.77\times10^{-8}$ | $8.62\times10^{-10}$ | 1000 | 1000 | 7500 | 5400 |

the following, approximate key figures:

- Calcium hydroxide 2.00 g/g silica fume
- Chemically bound water 0 g/g silica fume
- Gel water 0. 5 g/g silica fume
- Total heat generation 565 kJ/kg silica fume

Using the hydration model and the stoichiometry of the reaction of silica fume proposed by Maekawa et al.[10] and Lura[11], the amounts of calcium hydroxide, chemically bound water and capillary water in cement-silica-fume blends during hydration can be determined using the following equations:

(9)

$$W_{cap} = W_0 - 0.4\times C_0\times\alpha - RCW_{SF}\times\alpha_{SF}\times P - RPW_{SF}\times\alpha_{SF}\times P \quad \text{----} \quad (10)$$

$$W_{cbm} = v\times C_0\times\alpha + RCW_{SF}\times\alpha_{SF}\times P \quad \text{----} \quad (11)$$

In Eqs. (9), (10) and (11), $CH$, $W_{cap}$ and $W_{cbm}$ are the masses of calcium hydroxide, capillary water and chemically bound water, respectively; $\alpha_{SF}$ is the ratio between the released heat and the total heat generation of the silica fume; $P$ is the mass of the silica fume in the mixture proportion; $RCH_{CE}$ is the mass of calcium hydroxide produced from the hydration of cement; $RCH_{SF}$ is the mass of reacted calcium hydroxide in the reaction of silica fume; $RCW_{SF}$ is the mass of chemically bound water in the reaction of silica fume; and $RPW_{SF}$ is the mass of gel water in the reaction of silica fume.

Due to the high specific surface area and great pozzolanic activity of SF, it is assumed in the present paper that the hydration of SF involves two processes: a phase-boundary reaction process and a diffusion process. The hydration equation of silica fume can be written as follows:

$$\frac{d\alpha_{SF}}{dt} = \frac{m_{CH}(t)}{P}\frac{3\rho_w}{v_{SF}r_{SF0}\rho_{SF}} \frac{1}{\frac{r_{SF0}}{D_{eSF}}(1-\alpha_{SF})^{\frac{-1}{3}} - \frac{r_{SF0}}{D_{eSF}} + \frac{1}{k_{rSF}}(1-\alpha_{SF})^{\frac{-2}{3}}} \quad \text{---(12-1)}$$

$$D_{eSF} = D_{eSF0}\times\ln(\frac{1}{\alpha_{SF}}), \quad \text{----------} \quad (12-2)$$

where $m_{CH}(t)$ (kg/$m^3$) is the mass of calcium hydroxide in a unit volume of hydrating cement-silica-fume blends, which can be obtained from Eq. (9); $P$ (kg/$m^3$) is the silica-fume mass in the mixing proportion; $v_{SF}$ is the stoichiometric ratio of the mass of CH to silica fume; $r_{SF0}$ is the radius of a silica fume particle; $\rho_{SF}$ (g/$cm^3$) is the density of the silica fume; $D_{eSF0}$ ($cm^2$/h) is the initial diffusion coefficient; and $k_{rSF}$ (cm/h) is the reaction-rate coefficient.

The effect of temperature on the silica-fume reaction is considered to follow the Arrhenius law as follows:

$$D_{eSF0} = D_{eSF20}\exp(-\beta_{3SF}(\frac{1}{T}-\frac{1}{293})) \quad \text{-----} \quad (12-3)$$

$$k_{rSF} = k_{rSF20} \exp(-\frac{E_{SF}}{R}(\frac{1}{T} - \frac{1}{293})) \text{ ,----- (12-4)}$$

where $D_{eSF20}$ and $k_{rSF20}$ are the values of $D_{eSF}$ and $k_{rSF}$ at 293 K, respectively, and $\beta_{3SF}$ (K) and $E_{SF}/R$ (K) are the temperature-sensitivity coefficients of $D_{eSF}$ and $k_{rSF}$, respectively.

The released heat of the hydrating blends consists of the heat released from Portland-cement hydration and the heat released from the mineral-admixture reaction. The total released heat is expressed by Eq. (13-1):

$$\frac{dQ}{dt} = C_0 \times \sum g_i H_i \frac{d\alpha}{dt} + P \times H_{SF} \times \frac{d\alpha_{SF}}{dt} \text{ ,---- (13-1)}$$

where the first term derives from the hydration of Portland cement and the second derives from the reaction of the silica fume; $H_{SF}$ is the total heat generation content of the silica fume (by comparing the analytical and experimental data, Maekawa et al.[10] set the total heat generation of silica fume to 565 kJ/kg). (It should be noted that the silica-fume-reaction model, Equations 9-13 in section 2.2, is the original work of the author. Equations 9-13 are originally proposed to describe the pozzolanic reaction of silica fume and the heat-evolution rate of silica-cement blends. The stoichiometry of the pozzolanic reaction of silica fume is adopted from references[10,11].)

## 3. Prediction of temperature history in the hardening of ultra-high performance concrete

### 3.1 Evaluation on the calcium hydroxide contents in UHPC

Nguyen[12] carried out experimental investigations of the development of the properties of silica-fume-blended ordinary concrete and ultra-high-performance concrete. Specimens with three water-to-binder ratios of 0.18, 0.25 and 0.40 and various amounts of silica-fume additions, from 10 to 30%, were cured at 20℃. The calculated Bogue composition for cement is 63.77% $C_3S$, 9.24% $C_2S$, 8.18% $C_3A$ and 9.13% $C_4AF$. The specimens with water/binder ratios of 0.25 and 0.4 (paste specimens) were sealed for curing with a plastic lid, and the specimens with water/binder ratio of 0.18 (UHPC specimen) were cured in a fog room until the day of testing. The mix proportions of the UHPC specimens are shown in Table 2. The imbibition of water from the surrounding fog environment is related to the chemical shrinkage of hydrating blends. For the specimens with water-to-binder ratios of 0.25 and

Table 2. Mixing proportions for UHPC

| Amount of cement (kg/m$^3$) | Water/binder ratio (by weight) | Sand/binder ratio (by weight) | SF (% by weight) | Superplasticizer (solid% by weight of binder) |
|---|---|---|---|---|
| 1010 | 0.18 | 1 | 0 | 0.9 |
| 885 | 0.18 | 1 | 10 | 0.6 |
| 765 | 0.18 | 1 | 20 | 0.7 |
| 645 | 0.18 | 1 | 30 | 1.25 |

Table 3. Reaction coefficients for the silica-fume-reaction model

| $k_{rSF20}$ (cm/h) | $D_{eSF20}$ (cm$^2$/h) | $E_{SF}/R$ | $\beta_{3SF}$ |
|---|---|---|---|
| $1.80\times10^{-9}$ | $1.92\times10^{-12}$ | 5000 | 7000 |

0.18, superplasticizer was used to achieve a flow value between 210mm and 230mm. The amount of calcium hydroxide (CH) in the samples was determined by TGA at different ages, i.e., 6 h or 1, 3, 7, 28 or 91 days.

Based on the amount of calcium hydroxide, the reaction coefficients $k_{rSF20}$ and $D_{eSF20}$ of the silica-fume-reaction model can be obtained and are shown in Table 3. It should be noted that the evaluated calcium hydroxide contents are derived from modeling and the experimental results are taken from the work of Nguyen[12].

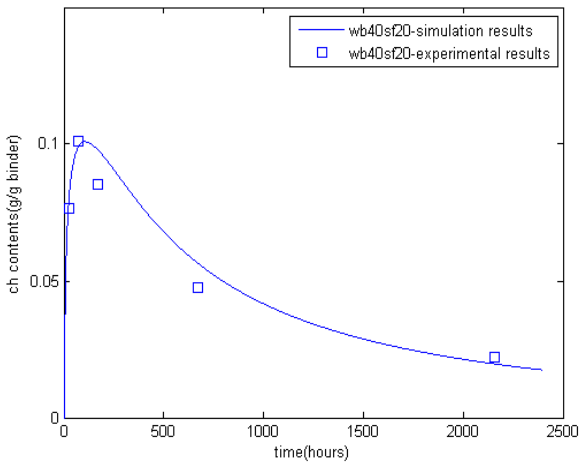


Figure 1-a. W/B 0.4 with 20% silica fume.

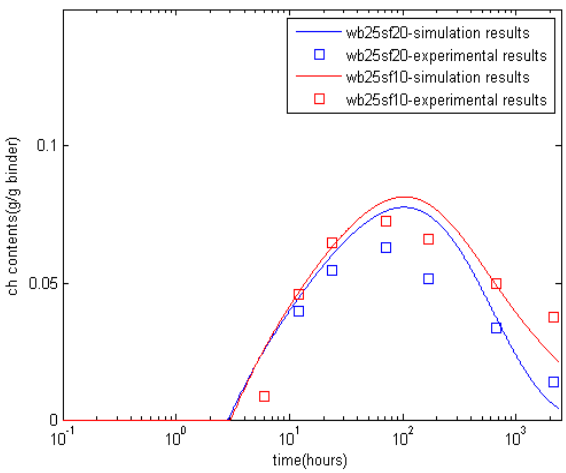


Figure 1-b. W/B 0.25 with 10% and 20% silica fume.

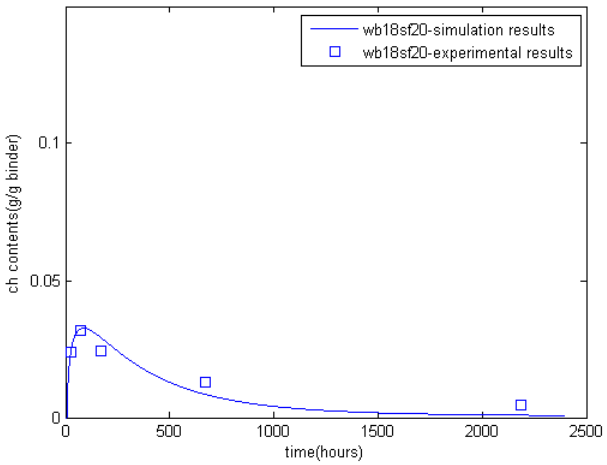


Figure 1-c. W/B 0.18 with 20% silica fume.

**Figure 1. Evaluation of the calcium hydroxide contents in silica-fume-cement paste.**

The evolution of the CH amount is shown as a function of the hydration time in Figure 1. As shown in Figure 1, the simulation results agree well with the experimental results overall. In the hydration of cement-silica-fume blends, the evolution of the amount of CH depends on two factors: the Portland-cement hydration that produces CH and the pozzolanic reaction that consumes CH. In the initial period, the production of CH is the dominant process, and in the later period, the consumption of CH is the dominant process. In the experimental range (the silica-fume replacement ratio ranges from 10% to 30%), the CH amount initially increases, reaches a maximum value and then decreases. The proposed model is valid for ultra-high-performance concrete (water-to-binder ratio: 0.18), high-strength concrete (water-to-binder ratio: 0.25) and ordinary-strength concrete (water-to-binder ratio: 0.4).

### 3.2 Evaluation of adiabatic temperature rise in silica-fume-blended concrete

In this part, the experimental results for the adiabatic temperature rise of silica-fume concrete[13] are used to verify the proposed model. The calculated

Table 4. Mix proportions for silica-fume-blended concrete

| Specimen | Cement (kg/m$^3$) | Water (kg/m$^3$) | SF (kg/m$^3$) | Aggregate(kg/m$^3$) | Super-plasticizer (kg/m$^3$) | Water/cement ratio | SF/cement ratio |
|---|---|---|---|---|---|---|---|
| WC30 | 529.5 | 158.9 | - | 1748.3 | 5.82 | 0.3 | - |
| WC30SF5 | 474.8 | 142.4 | 23.7 | 1800.4 | 5.7 | 0.3 | 0.05 |
| WC30SF10 | 483.9 | 145.2 | 48.4 | 1752.6 | 0.0 | 0.3 | 0.1 |
| WC30SF30 | 453.2 | 136.0 | 136.0 | 1679.9 | 0.0 | 0.3 | 0.3 |

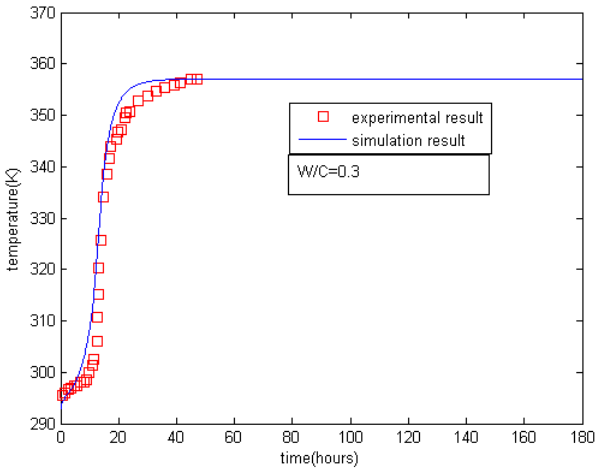


Figure 2-a. Adiabatic temperature rise of Portland-cement concrete with a water-to-cement ratio of 0.3

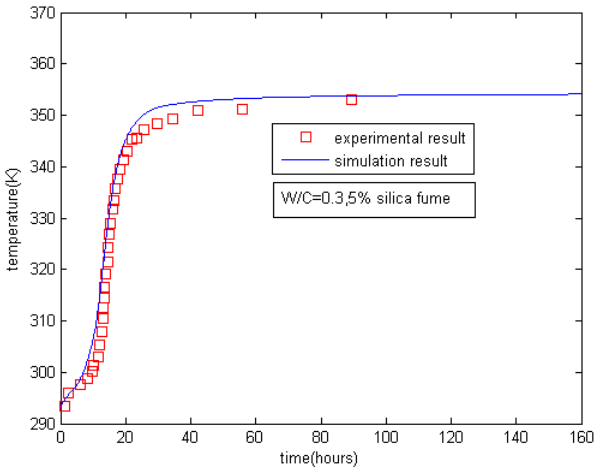


Figure 2-b. Adiabatic temperature rise of silica-fume-blended concrete with a water-to-cement ratio of 0.30 and 5% silica fume

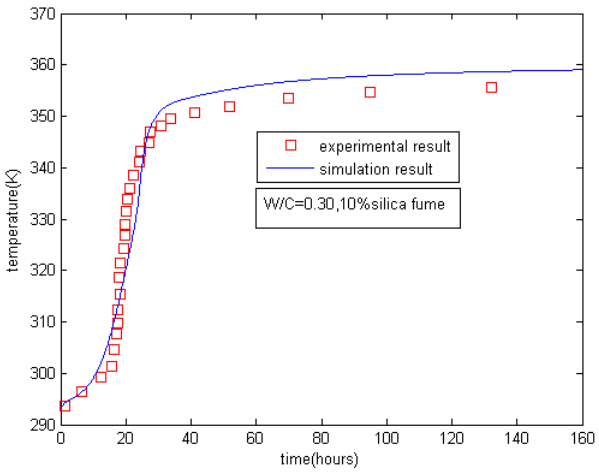


Figure 2-c. Adiabatic temperature rise of silica-fume-blended concrete with a water-to-cement ratio of 0.30 and 10% silica fume

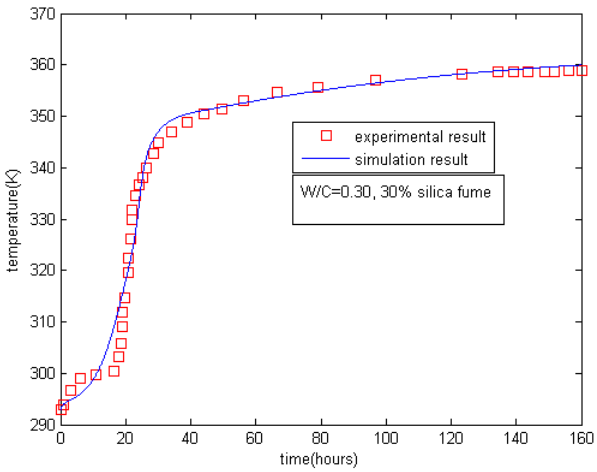


Figure 2-d. Adiabatic temperature rise of silica-fume-blended concrete with a water-to-cement ratio of 0.30 and 30% silica fume

**Figure 2. The comparison between the experimental results and the simulated results of the adiabatic temperature rise**

Bogue composition for cement is 57.1% $C_3S$, 15.3% $C_2S$, 7.7% $C_3A$ and 8.4% $C_4AF$. The mix proportions of silica-fume-blended concrete are shown in Table 4. The water-to-cement ratio of concrete is 0.3, and the silica-fume-replacement ratio ranges between 0.05 and 0.3. The mixtures are designed to be workable using a plasticizer. The incremental temperature at each time step under adiabatic conditions can be calculated as:

$$\Delta T = \frac{dQ(t)}{Cp(t)}, \quad \text{---------- (13-2)}$$

where $\Delta T$ is the incremental temperature in one time step; $dQ(t)$ is the released heat, which can be determined from Equation (13-1); and $Cp(t)$ is the heat capacity of concrete, which can be calculated by the sum of each component (cement, silica-fume aggregate, water and chemically bound water). When the superplasticizer is used in mixing the concrete, the initial dormant period will be prolonged. To fit the experimental results in the initial dormant period, the coefficient $B_{20}$, which is related to the initial dormant period of cement hydration, is multiplied by a factor of 0.2, whereas the other coefficients do not change. Based on the adiabatic temperature rise of the silica-fume-blended concrete, the temperature-sensitivity coefficients $\beta_{3SF}$ and $E_{SF}/R$ are calibrated and shown in Table 2. A comparison between the experimental results and the predicted results is shown in Figure 2. The predicted results generally agree with the experimental results. The proposed model can reflect the dependence of the reaction of silica fume on the calcium hydroxide.

When silica fume is incorporated into concrete, two possible reasons may be accepted to explain the change in the generation of the heat. One is the pozzolanic reaction of the amorphous silica in silica fume, and the other is the influence of the silica fume on the heat of cement hydration. In the current paper, a new model is proposed that can describe the pozzolanic reaction between calcium hydroxide and silica fume (section 2.2). On the other hand, the influence of silica fume on the heat of cement hydration is considered by looking at the amount of capillary water (Equation (10)) and the water-withdrawal mechanism (Equation (4)). Thus, the proposed model shows a strong ability to predict the development of the properties of silica-fume concrete, such as the temperature rise under adiabatic conditions.

### 3.3 Prediction of temperature history in the hardening of ultra-high-performance concrete

In construction sites, the curing temperature of concrete typically varies from location to location in each structure at each stage. For a typical thick member, the increase in the temperature at the core is much faster than that near the surface during the early stages of curing. To estimate the thermal stress and

strain, as well as to prevent thermal cracking, it is essential to predict the temperature distribution and history in quasi-adiabatic concrete. By combining the hydration model with a finite-element method (FEM), a numerical procedure is proposed that can be used to calculate the concrete-temperature distribution and history during hardening.

#### 3.3.1 The Equation Governing the Model

At any time, the temperature distribution in a hardening concrete is represented by a dynamic heat balance between the heat generated inside the concrete and the heat lost to the surroundings. The heat generation inside is due to the hydration reactions of the cement and the mineral admixtures. The temperature distribution is determined by the following heat equation[14]:

$$\rho C \frac{\partial T}{\partial t} = div(k \nabla T) + \frac{dQ}{dt}, \text{----------} \quad (14)$$

where ($\rho C$) is the heat capacity of the hydrating concrete and can be calculated as the sum of the individual components of concrete; $k$ is the thermal conductivity of the concrete; $T$ is the concrete temperature; $t$ is time; and $dQ/dt$ is the heat-generation rate in hardening concrete, which can be calculated based on the degrees of hydration of the cement and the mineral admixtures (Eq. (13)).

### 3.3.2 Boundary and initial conditions

Eq. (14) is subject to two types of boundary conditions. The first is that the temperature along the boundary or around a portion of the boundary is known and the second is that the energy transferred through the boundary is known. For ordinary engineering structures, the second type of boundary condition normally holds. This boundary condition can be described by the following equation:

$$k\nabla T = \beta(T_s - T_a), \quad \text{---------- (15)}$$

where $\beta$ is the heat-convection coefficient between the surface of the concrete and the surrounding environment; $T_s$ is the temperature on the surface of the concrete; and $T_a$ is the temperature of the surrounding environment.

The initial condition can be described by the following equation:

$$T|_{t=0} = T_0 \quad \text{---------- (16)}$$

where $T_0$ is the initial temperature of the concrete member.

### 3.3.3 Numerical Method for Solving the Governing Equation

In this paper, a finite-element method is adopted to solve Eq. (14). Eight-node isoparametric elements are built to model the volume of concrete in three-dimensional (3D) space. Following the 3D approximation, Eq. (14) can be rewritten as follows:

$$[B]\{T\} + [C]\frac{\partial\{T\}}{\partial t} = \{P\}. \quad \text{---------- (17)}$$

In Eq. (17), the global matrices $[B]$, $[C]$ and $\{P\}$ are obtained from the assembly of the element matrices as follows:

$$[B] = \sum_e [b]_{ij}^e \quad \text{---------- (18-1)}$$

$$[C] = \sum_e [b]_{ij}^e \quad \text{---------- (18-2)}$$

$$\{P\} = \sum_e [p]_i^e. \quad \text{---------- (18-3)}$$

Furthermore, based on numerical time integration, Eq. (17) can be written as follows:

$$\begin{aligned}&(\frac{1}{\Delta t}[C] + \theta[B])\{T\}_{n+1} \\ &= (\frac{1}{\Delta t}[C] - (1-\theta)[B])\{T\}_n + \{P\}_n\end{aligned}. \quad \text{---------- (19)}$$

Generally, the value of the parameter $\theta$ should be greater than 0.5 to ensure the stability of the numerical integration. In this paper, based on the Galerkin method in the time domain, the value of the parameter $\theta$ is determined to be 2/3[14].

Prediction of Temperature Distribution in the Hardening of Ultra-high-performance Concrete

Maruyama et al[15]. conducted an experimental investigation on the temperature distribution in ultra-high-performance concrete. The mix proportions of concrete are shown in Table 5. Low-heat Portland cement was used (the calculated Bogue composition for the cement is 29.5% $C_3S$, 49% $C_2S$, 4% $C_3A$ and 9.5% $C_4AF$), and the water-to-binder ratio and silica-fume-replacement ratio were 15% and 10.5%, respectively. The dosage of superplasticizer was determined to have a flow value of 60 cm, and the air content was determined to be 2%. A full-scale model column (a section of 900mm

Table 5. Mix proportions of ultra-high-performance concrete

| Water/binder ratio | Water ($kg/m^3$) | Cement ($kg/m^3$) | Silica fume ($kg/m^3$) | Sand ($kg/m^3$) | Gravel ($kg/m^3$) | Super plasticizer/binder (%) |
|---|---|---|---|---|---|---|
| 0.15 | 155 | 929.7 | 103.3 | 451 | 930 | 2.5 |

x900mm with a height of 1100mm) was equipped to measure the temperature history. The specimen was located in an enclosed experiment room. The change in the environmental temperature was recorded continuously throughout the entire experiment. Thermocouples were installed at the center and at a point 50mm above the surface to measure the temperature. The top and bottom surfaces of the specimen were thermally insulated with 100-mm-thick polystyrene foam, and the formworks in the surrounding four faces were metal molds. The thermal conductivity of the concrete was 1.5 W/(m · K), and the heat-transfer coefficient between the covered surfaces of the metal molds and the surrounding environment was 10 $W/(m^2 \cdot K)$ [15].

Finite-element modeling with 3D elements was used for the temperature analysis. Because of the symmetry of the geometry and the boundary conditions and initial conditions, the FEM mesh and calculation were only applied for one-eighth of the specimens. The boundary conditions of the symmetry planes were treated as insulated boundary conditions. As shown in Figure 3, for the analytical discretization of the concrete specimen, 891 (9×9×11=891) eight-node brick elements were used. In the modeling procedure, the concrete column was first divided into discrete elements, and the heat-evolution rate of each element in one time step was calculated using a hydration model based on the current element temperature.

Figure 4 compares the experimental results and the analysis results of the finite-element modeling. The analysis results generally reproduce the experimental temperature history. The maximum temperature at the center of the specimen reached 60℃ from an initial temperature of 23℃. It is noteworthy that the dormant period, which is reflected by the sudden increase in temperature, is quite prolonged. The sudden increase in temperature occurred approximately 24 h after casting, when conventional concrete shows a peak in temperature. This phenomenon can be explained by the addition of the superplasticizer, which has a delayed effect on the hydration of cement.

The temperature distribution and temperature history during the hardening of concrete depends on factors such as the heat evolution of hydration, the geometry of the structural members, the initial conditions and the boundary conditions. The value of this work lies in the determination of the heat evolution through a hydration model that considers both the cement hydration and the reaction of the mineral admixtures. Mutual interactions between the cement hydration and the reaction of the mineral admixtures are considered based on the amount of capillary water and the amount of calcium hydroxide remaining in the system. This model can also be integrated into other commercial software as a module for predicting the properties of hardening blended concrete.

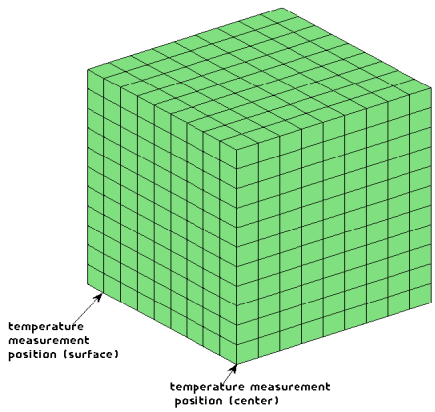


Figure 3. Finite-element meshing of the concrete specimen

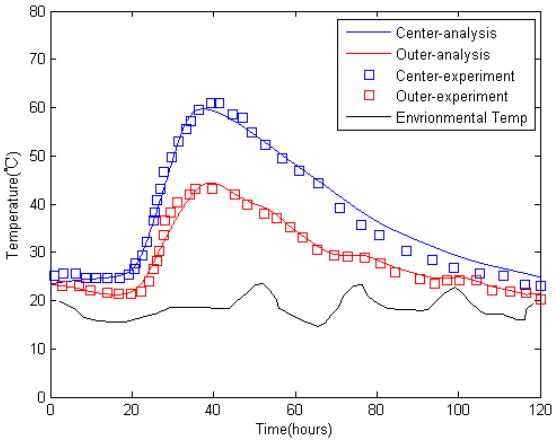


Figure 4. Temperature history during the hardening of ultra-high-performance concrete

## 4. Conclusions

This paper presents a numerical procedure to predict the temperature history of ultra-high-performance concrete. This numerical procedure starts with a hydration model that considers both the hydration of the cement and the pozzolanic reaction of the silica fume. The interactions between the hydration of the cement and the pozzolanic reaction of the silica fume are considered through the amount of calcium hydroxide and capillary water. The proposed hydration model has considered the effects of the water-to-binder ratio, the silica-fume-replacement ratio and the curing temperature on the heat-evolution rate of hydrating blends. Furthermore, in the finite-element procedure, the heat-evolution rate of each element in one time step was calculated using the hydration model based on the current element temperature. The results of the analysis of temperature history in ultra-high-performance concrete agree well with the experimental results.

## Acknowledgements

This research was supported by a grant (13SCIPA02) from Smart Civil Infrastructure Research Program funded by Ministry of Land, Infrastructure and Transport (MOLIT) of Korea government and Korea Agency for Infrastructure Technology Advancement (KAIA).

## References

1. Graybeal B, Tanesi J. Durability of an Ultra high-Performance Concrete. Journal of Materials in Civil Engineering. 2007 Oct;19(10):850-4.
2. Wang C, Dilger WH. Prediction of temperature distribution in hardening concrete. In: Spingenschmid R, editor. Proceeding of Thermal Cracking in Concrete at Early Ages; 1994 Oct 10-12; London, London: RILEM; 1995. p.21-8.
3. Cook WD, Aitcin PC and Mitchell D. Thermal Stresses in Large High-Strength Columns. ACI Materials Journal. 1993 Feb;89(1):61-8.
4. Swaddiwudhipong S, Shen D, Zhang MH. Simulation of the exothermic hydration process of Portland cement. Advances in cement research. 2002 Apr;14(2):61-9
5. Tian Y, Jin X, Jin N. Thermal cracking analysis of concrete with cement hydration model and equivalent age method. Computers and Concrete. 2013 Apr;11(4):271-89
6. De Schutter G. Hydration and temperature development of concrete made with blast-furnace slag cement. Cement and Concrte Research. 1999 Jan; 29(1):143-9.
7. De Schutter G, Taerve L. Degree of hydration-based description of mechanical properties of early age concrete. Materials and Structures. 1996 Jul; 29(6):335-44.
8. Tomosawa F. Development of a kinetic model for hydration of cement. In: Chandra S, editor. Proceedings of tenth international congress chemistry of cement; 1997 Jun 2-6; Gothenburg, Gothenburg; Amarkai AB and Congrex Goteborg AB; 1997. p.51-58.
9. Wang XY, Lee HS, Park KB , Kim JJ , Golden JS. A multi-phase kinetic model to simulate hydration of slag-cement blends. Cement & Concrete Composites. 2010 Jul; 32(6):468-77
10. Maekawa K, Chaube R, Kishi T. Modeling of concrete performance: hydration, microstructure formation and mass transport. London and New York: ROUTLEDGE ;1998. 308 p.
11. Lura P, Jensen OM, Breugel K. Autogenous shrinkage in high-performance cement paste: An evaluation of basic mechanisms. Cement and Concrete Research. 2003 Feb; 33(2):223-32

12. Nguyen VT. Rice Husk Ash as a Mineral Admixture for Ultra High Performance Concrete [dissertation]. Netherlands: Delft University of Technology; 2011. 183 p.
13. Bentz DP, Waller V, Larrard F. Prediction of adiabatic temperature rise in conventional and high performance concretes using 3-D microstructural model. Cement and Concrete Research. 1999 Feb;28(2):285-97
14. Daryl LL. A first course in the finite element method. 3rd ed. Pacific Grove: Brooks/Cole; 2002. 696p.
15. Maruyama I, Suzuki M, Sato R. Prediction of Temperature in Ultra High-Strength Concrete Based on Temperature Dependent Hydration Model. In: Henry G. Russell, editor. ACI SP-228, Proc. of 7th Int. Symp on High Performance Concrete. Washington DC:ACI; 2005. p.1175-86.